Bioconvection Casson Nanofluid Flow with Darcy-Forchheimer over a Permeable Stretching Sheet with Heat Source and Chemical Reaction

Muhammad Iqbal *

Posted Date: 4 March 2025

doi: 10.20944/preprints202503.0250.v1

Keywords: Casson Nanofluid; Bioconvection; Porous Media; Gyrotactic Microorganisms; Stretching Sheet; Homotopy Analysis Method

Article

Bioconvection Casson Nanofluid Flow with Darcy-Forchheimer over a Permeable Stretching Sheet with Heat Source and Chemical Reaction

Muhammad Iqbal

Department of Mathematics, Division of Science and Technology, University of Education, Lahore 54000, Pakistan; m.iqbalbsf1703522@gmail.com

Abstract: In this paper, it analyses the phenomena of Casson fluid flow, including the complex interactions between permeation, viscous dispersion, Darcy-Forchheimer implications, heat source, chemical reaction, and the heat boundary layer. The behaviour of a two-dimensional continuous stream comprising gyrotactic microbes of bioconvection Casson nanofluid through a stretchy membrane that is warmed and permeable are investigated in this study. A collection of independent partial differential equations is converted into a set of non-linear ordinary differential equations by using the proper conversion system. The analytical assessment of the current work is done using the homotopy analytic strategy. The relevant parameters are visually demonstrated to impact the concentration of nanoparticles, temperature, velocities, and gyrotactic microorganism profiles. Mathematica tool is used to calculate findings and visuals. The results of this research are extremely important regarding real-world uses for chilling and also for academic advances in the mathematical modeling of Casson liquid motion with thermal exchange in engineering structures. The body's friction coefficient, mobile microbes, Sherwood number, and Nusselt coefficient are calculated. A comparison study between the shooting and HAM findings is carried out as well.

Keywords: Casson Nanofluid; Bioconvection; Porous Media; Gyrotactic Microorganisms; Stretching Sheet; Homotopy Analysis Method

1. Introduction

Newton's principles can be used to classify liquids into two primary groups: Newtonian and non-Newtonian. The reality that fluids that are not Newtonian are not subject to the Newtonian rule of viscosity sets them apart from Newtonian liquids. Non-Newtonian fluids have the potential to produce an irregular relationship between shear stress and shear rate due to the intricacy of their design and aftercare under the power type model, as show in Figure 1.

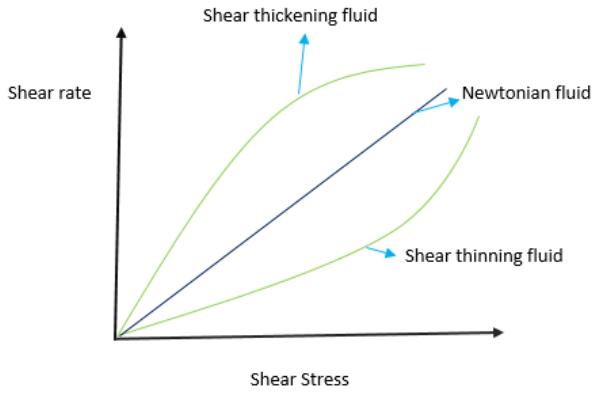

Figure 1. illustrates the non-Newtonian fluid model against shear stress and strain.

 doi:10.20944/preprints202503.0250.v1

For the past few years, researchers have been examining the flow of non-Newtonian fluids inside the boundary layer. Excitement generated by studies on non-Newtonian fluids in recent decades. A few notable instances of non-Newtonian content include sauce, paints, bloodstream at extremely small shear rates, lubricant representatives, sludge, chilling liquids, hydraulic representatives, and cleanliness products.This study focused on the Casson liquid design with multiple liquid models. A unconventional fluid with pseudo plastic characteristics is called a Casson fluid. The Casson model is a particular type of polymer liquid emulation that has several unique features, including a strong viscosity at high compression conditions, an elastic threshold, and shear thinning behavior. The Casson fluid acts like a solid substance as the stress placed on it exceeds the point of yield pressure. A potassium paginate sphere was carried over a Casson nanofluid that demonstrated MHD and convection from nature, according to Alwawi et al. [1]. Mukhopadhyay [2] investigated the effects of thermal transmission on the Casson liquid that is produced when an inflated sheet is exposed to blowing and suction. The effects of stretched surfaces and the Casson fluid movement on the field of magnets were examined by Mabood et al. [3]. They are currently examining the consequences of heat transmission when the outer layer is porous. The study conducted by Shah et al. [4] compared radiative electrically conductive Casson nanofluid. They claim that the liquid shear stress value reduces when the Casson liquid factor is enhanced. Puneeth et al. [5] examined the gyrotactic microorganisms' Casson fluid properties. In a setting with a combination of convection and fluctuating conductivity, Nadeem et al. [6] established a structure for the effect of viscosity on dissipating in Casson nanofluid streams. To examine how the mass distribution of heat influences the velocity of a dissipative Casson wet sheet, Alali et al [7] used a shooting computational approach. Employing the homotopy analytic technique, Dawar et al. [8] showed the magnetic Casson liquid streams containing microbes passing an extended cylinder. Using an MHD radiation chemical response with an upward appearance, Mkhatshwa et al. [9] researched the bioconvective Casson tiny particle mobility.

The Forchheimer (1901) model is applied to the momentum balance in order to account for the potential inertial flow effects caused by the shrinking of holes by damage to formation. The passage of a liquid across a material having linked gaps is known to be liquid circulation in a porous medium. Multiple uses refer to the Darcy-Forchheimer movement in porous media and thermal transfer measurement. Porosity medium can be made artificially (draws, insulation, catalytic pellets) or organically (wood, sponges that are sand beds, rocks). The number of connections and twisting pathways of empty areas, as well as other aspects of the porosity material framework, all influence the stream of the liquid. Hydro-geology, chemical engineering, ecological science, freshwater utilization, and gas-cleaning filtering all depend on a comprehension of and study of liquids moving in porous materials. The liquid and the medium that is porous interact according to the laws of liquid movement, most specifically Darcy's rule [10], which describes the connection among the motion of the liquid, variations in stress, and the medium's degree of porosity. Li et al. [11] explored the influence of chemical responses on the transport of MHD. Darcy Forchheimer compressed Casson liquid via an upright pipe. The Hamilton-Crosser system and the entropy-optimised Darcy-Forchheimer stream on the interface layer were examined by Nayak et al. [12].Casson fluid circulation with chemical responses in a Darcy-Forchheimer medium has been examined by Bilal et al. [13]. Naz et al. [14] looked into the heat transport and the creation of entropy in stratified MHD Carreau-tiny fluids containing gyrotactic bacteria. Additionally, they investigated the movement of Eyring-Powell substances across a spinning disc containing floating microbes in terms of temperature and species [15]. Rasool et al. [16] carried out a computational investigation of Darcy-Forchheimer and EMHD tiny liquid streams in permeable environments.

Bioconvection is the ability of one living thing or colony of microorganisms to migrate. The bio fuel biotechnology industry, as well as many other industrial and ecological systems, efficiently employ the physical implications of biological convection. Which finds extensive usage in the development of fuel cells, bioreactors, biodiesel, nuclear and medical engineering, and other fields of fuel, among

 doi:10.20944/preprints202503.0250.v1

others. The term "microorganism" refers to any type of organism that is too small to be identified separately. Swimming microorganisms, as shown in Figure 2. Green algae, viruses, bacteria, yeast, and protozoa are examples of the features of microbes. When microbes travel in a fluid, bioconvection occurs, leading to instabilities and a porous structure.

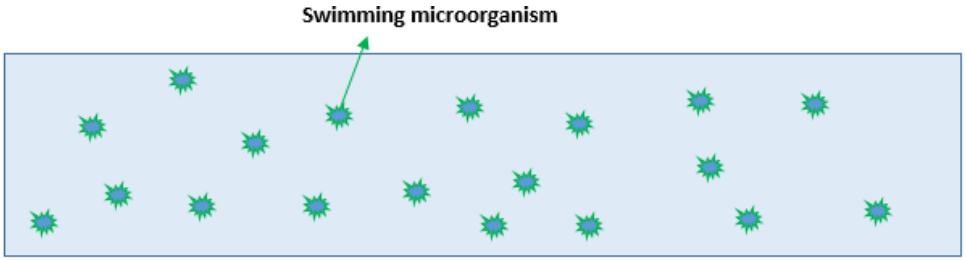

Figure 2. displays the swimming microorganisms.

The investigation of bioconvection between microorganisms and nanofluid is important for the production of currently available bionanomaterials. The present experiments utilizing bioconvection in nanofluids have attracted the interest of multiple experts and researchers. Gyrotactic organisms' bioconvection on thermosolutal convection caused by Marangoni across a sloped interface was studied by Kairi et al. [17]. On the MHD radiation chemical response to an upward appearance, Mkhatshwa et al. [18] assessed the bioconvective Casson liquid stream. Farooq et al. [19] conducted a 3-D bioconvection flow evaluation on a wider surface that included moving microbes, thermal radiation, and solutal boundary circumstances.Mahdy [20] conducted research on the convection-free circulation of an adiabatic upright conical in a tiny liquid, permeable material consisting of nanoparticles and gyrotactic organisms. Nineteen Giri et al. [21] investigated the impact of Stefan Fanning on the hydro-magnetic biological flow of liquid that travels via a permeable surface that contains gyrotactic microbes. Involving the transpiration motion of viscoelastic tiny particles, Waqas et al. [22] assessed the second-order slide implications, stimulation, and mass and heat transfer models with the dissolving mechanism. The Oldroyd-B nanofluid's bioconvection mobility in a porosity domain, including heat transmission, was studied by Khan et al. [23]. Sources [24–28] contain a few more studies on bioconvection.

The construction and operation of equipment used in the chemical industry, food processing, glass manufacturing, blood pumping, and various other industries all significantly rely on homogeneous or heterogeneous chemical responses. Homogeneous-heterogeneous reactions, such as those that occur in burning, catalysts, and biological structures, are the most common types of chemical responses. Many different uses in industries, including the preparation of food, polymers and pottery, hydro-metallurgy, freezing-damaged crops, citrus groves, atmospheric movements, pollution of the environment, and dry cooling and precipitation movements, rely on chemical reactions for their operations.Using the shooting approach for the computational study, Sajid et al. [29] investigated the MHD Blasus motion with chemical procedures and heat effect. The chemical responses of tiny fluids in a porous framework with changeable magnetism and heat transmission were studied by Sravanthi et al. [30]. In this case, heat transfer is significantly impacted by non-linear thermal radiation as opposed to linear thermal radiation. In a new framework for thermal insulation and turbulent viscosity, Alzahrani et al. [31] examined the Oldroyd-B tiny liquids through a permeable barrier with chemical processes, thermosolutal Marangoni conduction, and warmth source/sink. Chemically responsive impacts were applied over a needle by Mabood et al. [32]. Ramzan et al. [32] looked at the chemical process stimulant on the liquid flowing via a needle in a flow mechanism. There has only been one description of the MHD running for particles on a horizontal plane, by Makind [33]. A link has been made between the results of a chemical response and the movement of a Casson fluid over an object by Khan et al. [34]. Some others studies using chemical reactions in references [35–41].

 doi:10.20944/preprints202503.0250.v1

The term "nanofluid" refers to the element base liquid that has been infused with nanoparticles, as illustrated in Figure 3.

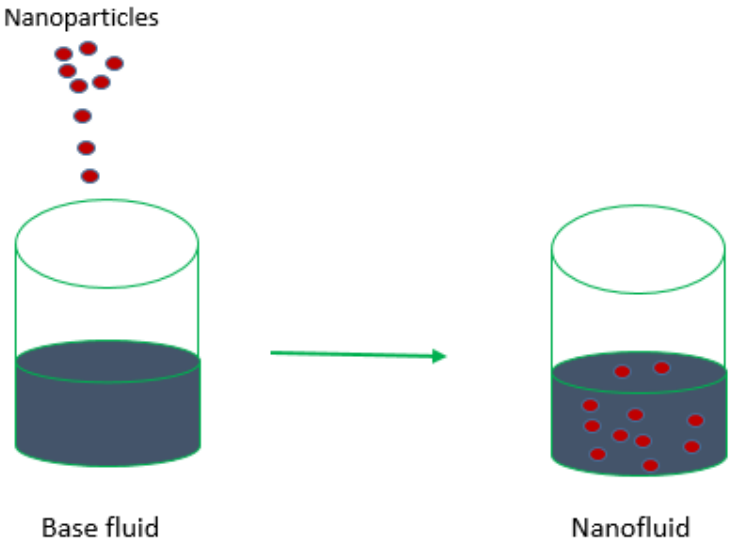

Figure 3. shows the suspension of nanoparticles and base fluid.

Nanofluid is an amalgam of fundamental fluids with nanomaterials. Nanofluids have superior thermal transmission properties and have several scientific and industrial uses. They are employed in climate control, cooling, airflow, and solar power plants, as well as for cooling and heating applications. There are several applications of nanofluids in solar energy technology, food, leather, automobiles, and nuclear power industries, as well as heat transfer devices and the cooling of electrical and vehicle systems, as expressed in Figure 4.

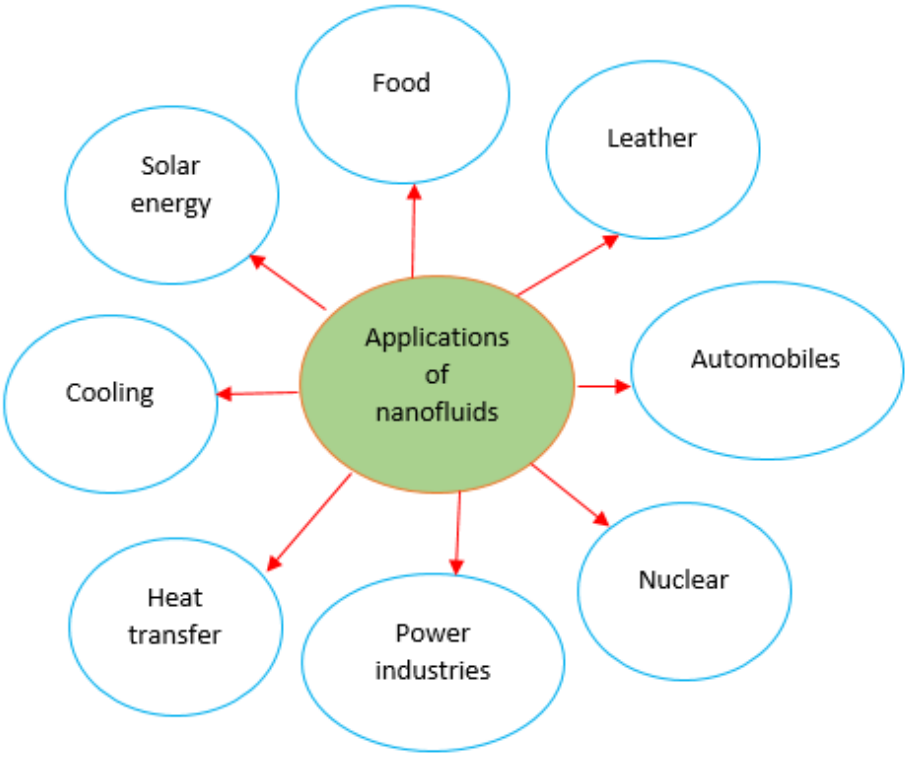

Figure 4. demonstrating the applications of nanofluids.

 doi:10.20944/preprints202503.0250.v1

In their studies, Khan et al. [42] introduced the model of bioconvective mass and warmth fluxes with stimulation energy and radiant heat, as well as the Cattaneo-Christov cross-diffusion movement of magnetized sticky nanofluid across cones, wedges, and sheets beneath convective boundary circumstances. Williamson nanofluid convective flow across the cone and wedges over changing non-isosolutal and nonisothermal circumstances was explored by Dawar et al. [43], who demonstrated the flow velocity is more intense on the cone than the sword. In the colloidal mixing of fluid with flake aluminum oxide, sphere nanotubes, and cylinder graphite, Cae. [44] found compelled, unrestricted, and hybrid convection. Alrabaiah et al. [45] used an adaptive continuing approach to study the silver-magnesium dioxide hybrid nanofluid that circulates within the cylindrical junction of the disc and dome, employing gyrotactic germs. Nazir [46] examined the hybrid nanofluid according to Carreau-Yasuda, passing through a porosity spinning funnel while accounting for viscosity dissolution, the production of heat, heating via Joules, generalized Ohm's rule, and Hall and ionization slip pressures. Shahid et al. [47] solved the MHD flow problem with nanofluid, including gyrotactic microbes, via a permeable layer using Chebyshev wavelength matching techniques. References [48–63]include information on the nanofluids and additional research.

In 1856, Darcy conducted the first investigation into the law of water flow in the ground. Darcy's law is a term used to describe how quickly a fluid passes through a porous material.

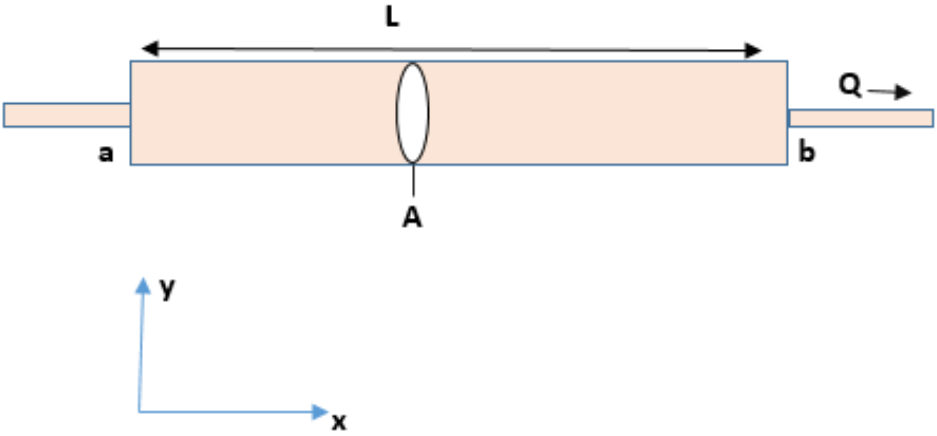

Figure 5. expresses the Darcy law.

This rate is directly related to the vertical elevation decrease between two locations in the medium and inversely proportional to the gap among them, according to the law. The way fluids flow through porous substances in reaction to a gradient of pressure is explained by Darcy's law. According to Darcy's law, the fluid must be incompressible, the flow must be laminar, and the porous media must be homogeneous and isotropic. In hydrogeology and reservoir engineering, it serves as the foundation for more intricate models and equations and offers a simpler depiction of the movement of fluid through porous medium.

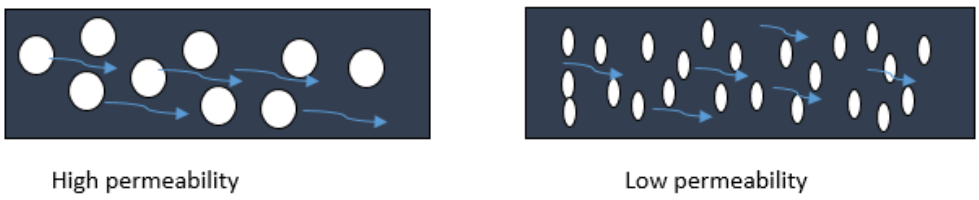

Figure 6. shows the difference between high and low permeability.

Ali et al. [64] examined the Casson nanofluid flow over an irregularly declining surface using the Darcy–Forchheimer model. The purpose of their investigation was to examine the effects of viscous

 doi:10.20944/preprints202503.0250.v1

dissipation and slip conditions on flow behaviour. A study by Kavita et al. [65] examined the effects of heat and mass transfer on the Darcy–Forchheimer Casson fluid movement over a non-permeable curved stretched sheet. Modified electroosmosis Hafeez et al. [66] Darcy–Forchheimer the movement of Casson nanofluid across expanding sheets with Newtonian heating.

This work is unique because it presents an analysis of the phenomena of Casson fluid flow, including the complex interactions between permeation, viscous dispersion, Darcy-Forchheimer implications, heat source, chemical responses, and heat boundary layer. Since prior research has offered fundamental understandings of Casson fluid flow, including gyrotactic microorganisms and porous mediums, this research contributes to the field by originally integrating these elements. The main objective of the current study is to examine the details of a two-dimensional constant motion consisting of an inflexible viscous bioconvection Casson fluid through a stretching surface that is quickly heat transmitted in porous media. Unlike Darcy's Law, Forchheimer's Law is used in the present framework to account for the non-linear resistance that increases in significance with higher movement. The system of boundary layer flow across a stretching sheet is now part of the research scope due to the rapid advancements in several scientific and technological domains. The results of this work are highly significant in terms of practical engineering cooling applications as well as theoretical advances in the mathematical modeling of Casson fluid flow with heat mass transfer in engineering systems. Its application in the geophysical sciences, biological engineering, oil reserve operations, biochemical and nuclear research, and other domains.

Novelty

The originality and novelty of the present experiment are that the HAM tool is applied to organize an analytical solution for Casson nanomaterial flow of mass and heat transfer produced from a stretching sheet with bioconvection, porosity, random motion, heat source, chemical reaction and thermomigration impacts. The novel outcomes offer a better perception of the flow of Casson fluid and heat transportation in the presence of bacteria, which will be helpful in multiple engineering and manufacturing applications such as biomedicine, biofertilizers, and industries. The research that follows offers answers to the following queries and includes a detailed realization of several mathematical and manufacturing processes.

- What is the influence of the magnetic field in bicoconvection Casson fluid?
- What is the consequence of Brownian movement, heat transfer, Darcy number and Fourchemmir principal on bioconvection in Casson liquid?
- How does the Casson fluid react in the presence of chemical reactions over the stretching sheet?

2. Mathematical Formulation

The circulation of blood in small arteries at minimal shear rates has been mathematically modeled by several investigators using the Casson fluid model. The Casson parameter is denoted by β, and the critical value is dependent on the non-Newtonian model. For constant movement, the following is the Casson fluid rheological equation [67–69]:

$$R_{ij} = \begin{cases} \tau_{ij} = \left(2\mu_1 + \frac{(2)^{\frac{1}{2}} p_y}{\pi^{\frac{1}{2}}}\right) e_{ij}, & \pi > \pi_c \\ \tau_{ij} = \left(2\mu_1 + \frac{(2)^{\frac{1}{2}} p_y}{\pi_c^{\frac{1}{2}}}\right) e_{ij}, & \pi < \pi_c, \end{cases} \tag{1}$$

 doi:10.20944/preprints202503.0250.v1

where $p_y = e_{ij}e_{ij}$ and $\beta = \frac{\mu_1(2\pi)^{\frac{1}{2}}}{p_y}$. π_c is the critical value as defined by a non-Newtonian framework, and π is an aspect of the deform rate. In the present work, modeled equations are given .

$$u\frac{\partial u}{\partial x} + v\frac{\partial u}{\partial y} = \nu_f\left(1 + \frac{1}{\beta}\right)\frac{\partial^2 u}{\partial y^2} - \left[\frac{\sigma B_0^2}{\rho}u - \frac{\mu}{k_p}u\right], \tag{2}$$

$$u\frac{\partial T}{\partial x} + v\frac{\partial T}{\partial y} = \frac{1}{\rho c_p}\frac{\partial}{\partial y}\left(k\frac{\partial T}{\partial y}\right) + \frac{\mu_1}{\rho c_p}\left(1 + \frac{1}{\beta}\right)\left[\left(\frac{\partial u}{\partial y}\right)^2 + \frac{u^2}{k_1}\right] + \frac{Fu^3}{\rho c_p k_1} + \frac{q}{\rho c_p}, \tag{3}$$

$$u\frac{\partial C}{\partial x} + v\frac{\partial C}{\partial y} = D_B\frac{\partial^2 C}{\partial y^2} + \frac{D_T}{T_\infty}\frac{\partial^2 T}{\partial y^2} - k_r[C - C_\infty], \tag{4}$$

$$u\frac{\partial N}{\partial x} + v\frac{\partial N}{\partial y} = \frac{bW_{ce}}{C_w - C_\infty}\left[\frac{\partial N}{\partial y}\frac{\partial C}{\partial y} + N\frac{\partial^2 T}{\partial y^2}\right] + D_n\left(\frac{\partial^2 T}{\partial y^2}\right), \tag{5}$$

A collection of the equations for Casson nanofluid movement that have been addressed previously. Boundary conditions as follows:

$$\left[\begin{array}{c} v = v_0, \quad u = u_w + \frac{\mu}{\mu_1}\left(1 + \frac{1}{\beta}\right)\frac{\partial u}{\partial y}, \quad -k = h_s\frac{(T_s - T)}{T_y}, \quad C = C_w, \quad N = N_w, \quad at \quad y = 0, \\ u \to \infty, \quad T \to T_\infty, \quad C \to C_\infty, \quad N \to N_\infty, \quad as \quad y \to \infty \end{array}\right]. \tag{6}$$

The descriptions of the associated similarities are as follows:

$$\left[\begin{array}{c} \xi = \sqrt{(\frac{a}{\nu})}y, \quad u = axf(\xi), -v = \sqrt{(a\nu)}\left(f'(\xi)\right), \quad \theta(\xi)T_w - T_\infty = T - T_\infty, \\ \phi(\xi)C_w - C_\infty = C - C_\infty, \quad \chi(\xi)N_w - N_\infty = N - N_\infty \end{array}\right]. \tag{7}$$

In the preceding equations, u, v represent the velocity components across the x, y directions. Where C is the fluid concentration, C_∞ is the ambient concentration, k_p is the thickness of the porous media, k indicates the thermal conductive property of the Casson fluid, F_r is the Forchheimer parameter, N_∞ is the surrounding fluid density, and β is the Casson parameter, D_B shows the fluid Brownian diffusion coefficient, B_0 denotes the magnetic field, N shows the concentration of microbes, N_∞ is the ambient concentration of microbes, β Casson fluid parameter, c_p is the specific heat at constant pressure, N_w is the reference concentration of microbes, C_w is the wall concentration, W_{ce} is the maximum cell swimming speed, b represents the chemotaxis constant, and μ is the dynamic viscosity of the fluid.

2.1. Physical Description of the Problem

The trend of a two-dimensional viscous bioconvection Casson fluid Darcy flow, comprising gyrotactic microorganisms past a permeable surface, is shown in Figure 7. In the present investigation, the y-axis is opposite to the path of the sheet, while the x-axis is horizontal along the stretching sheet. To take into consideration the existence of chemical reactions, viscosity dissolution, slip circumstances, and behavior of warmth exchange. The constant magnetic field $B_0 = (0, y)$ is taken across the y-direction. The T_∞ represents the fluid ambient temperature and T_w is the temperature on the surface of the stretching sheet. The concentration of gyrotactic microbes at the wall is N_w and the ambient concentration of the microorganisms profile is N_∞.

 doi:10.20944/preprints202503.0250.v1

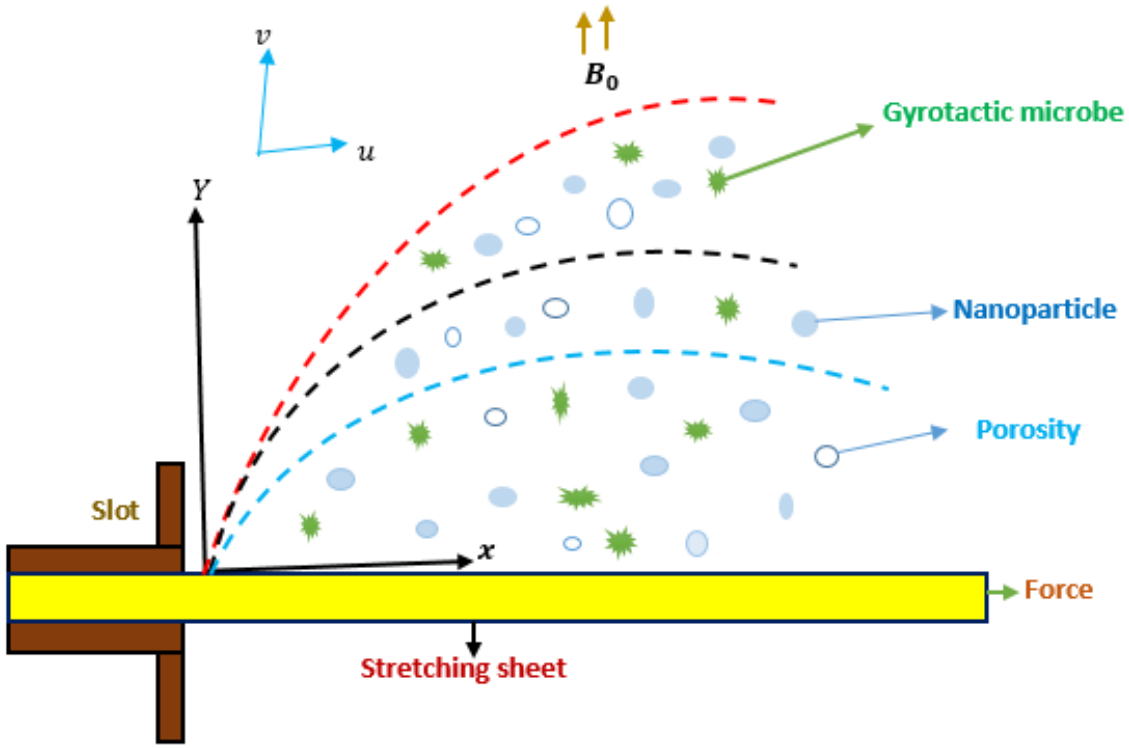

Figure 7. Flow geometry.

The resemblance transforms (7) are applied to turn the PDEs (2)–(5) with the boundary constraints (6) into a collection of ODEs. The devoid-of-dimensions structure of equations (2)–(5) is represented as

$$\left(1+\tfrac{1}{\beta}\right)f''+ff''-(f')^2-(M+P_m)f'=0, \tag{8}$$

$$Pr\Big((1+\Lambda_1\theta)\theta''+\Lambda_1(\theta')^2\Big)+f\theta'+Ec*e^{-a\theta}\left(1+\tfrac{1}{\beta}\right)\Big((f'')^2+D_a(f')^2\Big)+F_r(f')^3+Q_0=0, \tag{9}$$

$$Sc\phi''+\frac{Nt}{Nb}\theta''+f\phi'-S_r=0, \tag{10}$$

$$\chi''+Pe[\phi''\chi+\Omega\phi''+\chi'\phi']+Lb(f\chi')=0. \tag{11}$$

Boundary conditions as follows:

$$\begin{bmatrix} f(0)=1, & f'(0)=1+e^{-a\theta}\left(\frac{1+\beta}{\beta}\right)f'(0), & \theta'(0)=-Bi\left(\frac{1-\theta(0)}{1+\Lambda_1}\right), \\ \phi(0)=1, & \chi(0)=1, f(\infty)=0, & \theta(\infty)=0, \quad \phi(\infty)=0, \quad \chi(\infty)=0 \end{bmatrix}. \tag{12}$$

The different flow parameters are discussed here in a dimensionless format.

$$P_m=\frac{\mu}{ak_p}, \quad M=\frac{\sigma B_0^2}{a\rho}, \quad Pr=\frac{c_p\nu_f}{k}, \quad Ec=\frac{\nu_f}{\rho c_p(T_w-T_\infty)}, \quad D_a=\frac{x}{k_f}, \quad F_r=\frac{Fa}{\rho c_p k_f},$$
$$Sc=\frac{D_B}{\nu_f a}, \quad Nt=\frac{D_T}{a\nu_f}(T_w-T_\infty), \quad S_r=\frac{k_r}{a^2}, \quad Lb=\frac{\nu_f a}{D_n}, \quad Pe=\frac{bW_{ce}}{D_n}, \quad \Omega=\frac{N_\infty}{N_w-N_\infty}. \tag{13}$$

 doi:10.20944/preprints202503.0250.v1

Some of the physical factors related to the mechanism are the rate of mass transfer Sh_x, the energy exchange stream Nu_x, and the surface coefficient C_{f_x}. The following is a reduced expression corresponding to these quantities:

$$\sqrt{(Re_x)}Nu_x = -\theta'(0), \quad \sqrt{(Re_x)}Sh_x = -\phi'(0), \quad Nn = \chi'(0), \sqrt{(Re_x)}C_{f_x} = \left(1 + \frac{1}{\beta}\right)e^{-a\theta}f'(0). \tag{14}$$

3. Solution of the Problem by HAM

More complex regressive regular differential problems are solved using the homotopic analytic strategy. The several benefits of the HAM versus competing approaches are enumerated in the summary that follows. This method solves the problem in a convergent manner. There are no computation errors or measurement errors. Neither uniformity regulators nor baseline units are used in this method. HAM can be used with both modest and big variation schemes. With this method, an arrangement with strong or lower fundamental components may be used.

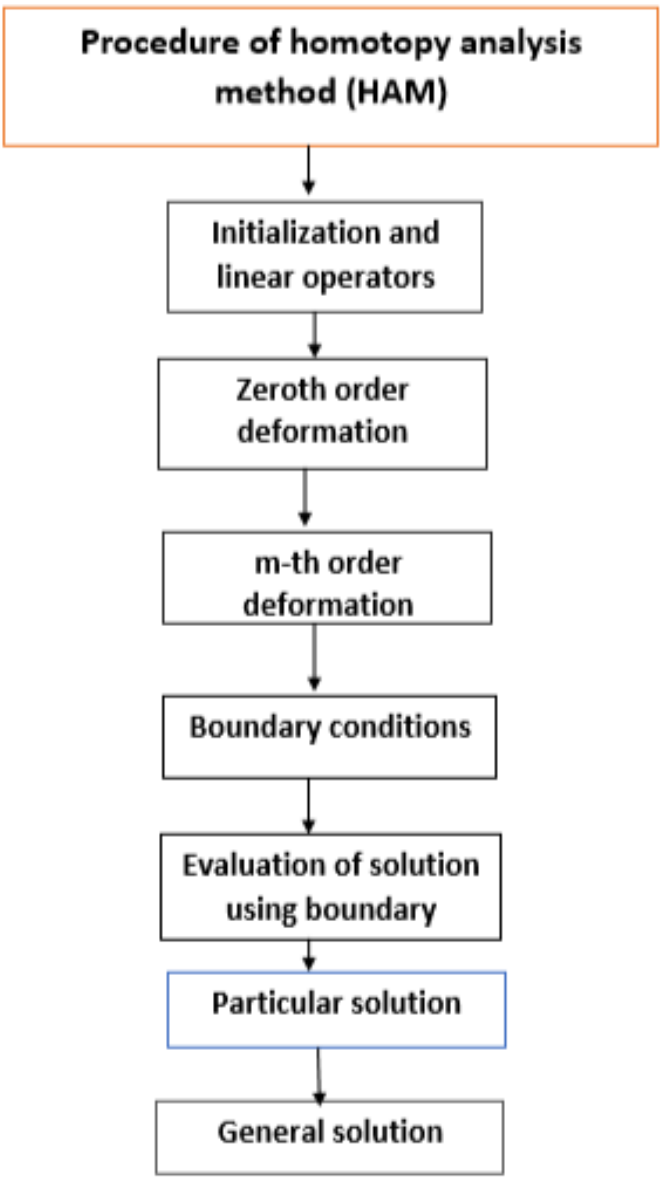

Figure 8. Flow chart of HAM.

 doi:10.20944/preprints202503.0250.v1

The fundamental assumptions and linear operators are considered to

$$f_0 = \lambda * 1 - \frac{1}{\exp^{\xi}}, \quad \theta_0 = \frac{Bi}{1+Bi} * \frac{1}{\exp^{\xi}}, \quad \phi_0 = \frac{1}{\exp^{\xi}}, \quad \chi_0 = \frac{1}{\exp^{\xi}}, \tag{15}$$

$$L_f = \frac{\partial^2 f}{\partial \xi^2} - f, \quad L_\theta = \frac{\partial^2 \theta}{\partial \xi^2} - \theta, \quad L_\phi = \frac{\partial^2 \phi}{\partial \xi^2} - \phi, \quad L_\chi = \frac{\partial^2 \chi}{\partial \xi^2} - \chi \tag{16}$$

$$\begin{aligned} L_f\Big(g_1 Exp(\xi) + g_2 Exp(-\xi)\Big) = 0, L_\theta\Big(g_3 Exp(\xi) + g_4 Exp(-\xi)\Big) = 0, \\ L_\phi\Big(g_5 Exp(\xi) + g_6 Exp(-\xi)\Big) = 0, L_\chi\Big(g_7 Exp(\xi) + g_8 Exp(-\xi)\Big) = 0, \end{aligned} \tag{17}$$

where g_1 to g_8 are the constants in the general approach.

3.1. Deformation Equations of Zeroth Order

$$(1-z)L_f\Big(f(\xi,z) + f_0(\xi)\Big) = z\hbar_f \aleph_f\Big(f(\xi,z)\Big), \tag{18}$$

$$(1-z)L_\theta\Big(\theta(\xi,z) + \theta_0(\xi)\Big) = z\hbar_\theta \aleph_\theta\Big(f(\xi,z), \theta(\xi,z)\Big), \tag{19}$$

$$(1-z)L_\phi\Big(\phi(\xi,z) + \phi_0(\xi)\Big) = z\hbar_\phi \aleph_\phi\Big(f(\xi,z), \phi(\xi,z), \theta(\xi,z)\Big), \tag{20}$$

$$(1-z)L_\chi\Big(\chi(\xi,z) + \chi_0(\xi)\Big) = z\hbar_\chi \aleph_\chi\Big(f(\xi,z), \phi(\xi,z), \chi(\xi,z)\Big), \tag{21}$$

where z is displayed as an underling parameter and $\hbar_f$, $\hbar_g$, $\hbar_\theta$, $\hbar_\phi$ and $\hbar_\chi$ are the non-zero additional variables. The nonlinear operators $\aleph_f$, $\aleph_\theta$, $\aleph_\phi$, and $\aleph_\chi$ are described as

$$\aleph_f(f(\xi,z)) = \Big(\tfrac{1+\beta}{\beta}\Big)\frac{\partial^2 f(\xi,z)}{\partial^2 \xi} + f(\xi,z)\frac{\partial^2 f(\xi,z)}{\partial^2 \xi} - \Big(\tfrac{\partial f(\xi,z)}{\partial \xi}\Big)^2 - \Big(M + P_m\Big)\frac{\partial f(\xi,z)}{\partial \xi}, \tag{22}$$

$$\begin{aligned} \aleph_\theta(f(\xi,z),\theta(\xi,z)) = Pr\Bigg[\Big((1+\Lambda_1\tfrac{\partial\theta(\xi,z)}{\partial\xi}\theta)\Big)\tfrac{\partial^2\theta(\xi,z)}{\partial^2\xi} + \Lambda_1\Big(\tfrac{\partial\theta(\xi,z)}{\partial\xi}\Big)^2\Bigg] + f(\xi,z)\frac{\partial\theta(\xi,z)}{\partial\xi} \\ + Ec * e^{-a\theta}\Big(\tfrac{1+\beta}{\beta}\Big)\Bigg[\Big(\tfrac{\partial^2 f(\xi,z)}{\partial^2\xi}\Big)^2 + D_a\Big(\tfrac{\partial f(\xi,z)}{\partial\xi}\Big)^2\Bigg] + F_r\Big(\tfrac{\partial f(\xi,z)}{\partial\xi}\Big)^3 + Q_0, \end{aligned} \tag{23}$$

$$\aleph_\phi(f(\xi,z),\phi(\xi,z)\theta(\xi,z)) = \frac{\partial^2\phi(\xi,z)}{\partial^2\xi} + \frac{N_t}{N_b}\frac{\partial^2\theta(\xi,z)}{\partial^2\xi} + f(\xi,z)\frac{\partial\phi(\xi,z)}{\partial\xi} - S_r, \tag{24}$$

$$\begin{aligned} \aleph_\chi(f(\xi,z),\phi(\xi,z),\chi(\xi,z)) = \frac{\partial^2\chi(\xi,z)}{\partial^2\xi} + Pe\Big(\tfrac{\partial^2\phi(\xi,z)}{\partial^2\xi}(\Omega + \chi(\xi,z) + \tfrac{\partial\chi(\xi,z)}{\partial\xi}\tfrac{\partial^2\phi(\xi,z)}{\partial^2\xi}\Big) \\ + L_b\chi(\xi,z)\frac{\partial f(\xi,z)}{\partial\xi}. \end{aligned} \tag{25}$$

Boundary constraints in the Equation (22)

$$f'(0,z) = 1 + e^{-a\theta(0,z)}\Big(1 + \tfrac{1}{\beta}\Big)f'(0,z), \quad f(0,z) = 1. \tag{26}$$

Boundary constraints in the Equation (23)

$$\theta'(0,z) = -Bi\Big(\tfrac{1-\theta(0,z)}{1+\Lambda_1}\Big), \quad \theta(\infty,z) = 0. \tag{27}$$

 doi:10.20944/preprints202503.0250.v1

Boundary constraints in the Equation (24)

$$\phi(0,z) = 1, \quad \phi(\infty,z) = 0. \tag{28}$$

Boundary constraints in the Equation (25)

$$\chi(0,z) = 1, \quad \chi(\infty,z) = 0. \tag{29}$$

For $z = 0$ and $z = 1$, Eqs. (22–25) become

$$z = 0 \Rightarrow f(\infty,0) = f_0(\infty) \quad and \quad z = 1 \Rightarrow f(\infty,1) = f(\infty), \tag{30}$$

$$z = 0 \Rightarrow \theta(\infty,0) = \theta_0(\infty) \quad and \quad z = 1 \Rightarrow \theta(\infty,1) = \theta(\infty), \tag{31}$$

$$z = 0 \Rightarrow \phi(\infty,0) = \phi_0(\infty) \quad and \quad z = 1 \Rightarrow \phi(\infty,1) = \phi(\infty), \tag{32}$$

$$z = 0 \Rightarrow \chi(\infty,0) = \chi_0(\infty) \quad and \quad z = 1 \Rightarrow \chi(\infty,1) = \chi(\infty). \tag{33}$$

Expanding $f(\xi, z)$, $\theta(\xi, z)$, $\phi(\xi, z)$ and $\chi(\xi, z)$ through Taylor series, Eqs. (34–37) generate

$$f(\xi,z) = f_0(\xi) + \sum_{m=1}^{\infty} f_m(\xi) z^m, \quad f_m(\xi) = \frac{1}{m!} \frac{\partial^m f(\xi,z)}{\partial \zeta^m} \Big|_{z=0}, \tag{34}$$

$$\theta(\xi,z) = \theta_0(\xi) + \sum_{m=1}^{\infty} \theta_m(\xi) z^m, \quad \theta_m(\xi) = \frac{1}{m!} \frac{\partial^m \theta(\xi,z)}{\partial \xi^m} \Big|_{z=0}, \tag{35}$$

$$\phi(\xi,z) = \phi_0(\xi) + \sum_{m=1}^{\infty} \phi(\xi) z^m, \quad \phi(\xi) = \frac{1}{m!} \frac{\partial^m \phi(\xi,z)}{\partial \xi^m} \Big|_{z=0}, \tag{36}$$

$$\chi(\xi,z) = \chi_0(\xi) + \sum_{m=1}^{\infty} \chi_m(\xi) z^m, \quad \chi_m(\xi) = \frac{1}{m!} \frac{\partial^m \chi(\xi,z)}{\partial \xi^m} \Big|_{z=0}. \tag{37}$$

From Eqs. (38), the convergence of the series is obtained by taking $z = 1$ for the appropriate values of $\hbar_f$, $\hbar_\theta$, $\hbar_\phi$ and $\hbar_\chi$, so

$$\begin{aligned} f(\xi) &= f_0(\xi) + \sum_{m=1}^{\infty} f_m(\xi), \quad \theta(\xi) = \theta_0(\xi) + \sum_{m=1}^{\infty} \theta_m(\xi), \\ \phi(\xi) &= \phi_0(\xi) + \sum_{m=1}^{\infty} \phi(\xi), \quad \chi(\xi) = \chi_0(\xi) + \sum_{m=1}^{\infty} \chi(\xi). \end{aligned} \tag{38}$$

3.2. m-th Order Deformation Problems

The m-th order deformation equations are

$$\begin{aligned} &L_f(f_m(\xi) - \delta_m f_{m-1}(\xi)) = \hbar_f \mathfrak{z}_m^f(\xi), \quad L_\theta(\theta_m(\xi) - \delta_m \theta_{m-1}(\xi)) = \hbar_\theta \mathfrak{z}_m^\theta(\xi), \\ &L_\phi(\phi_m(\xi) - \delta_m \phi_{m-1}(\xi)) = \hbar_\phi \mathfrak{z}_m^\phi(\xi), \quad L_\chi(\chi_m(\xi) - \delta_m \chi_{m-1}(\xi)) = \hbar_\chi \mathfrak{z}_m^\chi(\xi), \end{aligned} \tag{39}$$

$$\begin{bmatrix} f_m(0) = 0, & f_m(\infty) = 0, & \theta_m(0) = 0, & \theta_m(\infty) = 0, \\ \phi_m(0) = 0, & \phi_m(\infty) = 0, & \chi_m(0) = 0, & \chi_m(\infty) = 0 \end{bmatrix}, \tag{40}$$

where

$$\mathfrak{z}_m^f(\xi) = \left(1 + \tfrac{1}{\beta}\right) f''_{m-1} + \sum_{k=0}^{m-1} f''_{m-1-k} f'_k - \sum_{k=0}^{m-1} f'_{m-1-k} f'_k - (M + P_m) f'_{m-1}, \tag{41}$$

 doi:10.20944/preprints202503.0250.v1

$$\overset{\theta}{m}(\xi) = Pr\left(\theta''_{m-1} + \Lambda_1 \sum_{k=0}^{m-1} \theta''_{m-1-k}\theta_k + \Lambda_1 \sum_{k=0}^{m-1} \theta'_{m-1-k}\theta'_k\right) + \sum_{k=0}^{m-1} f_{m-1-k}\theta'_k + Ec * e^{(-a\theta')_{m-1}}$$

$$\left(1 + \frac{1}{\beta}\right)\left(\sum_{k=0}^{m-1} f''_{m-1-k}f''_k + D_a \sum_{k=0}^{m-1} f'_{m-1-k}f'_k\right) + F_r \sum_{k=0}^{m-1} f'_{m-1-k}f'_{k-1}f'_l + Q_0, \quad (42)$$

$$\overset{\phi}{m}(\xi) = Sc\phi''_{m-1} + \frac{N_t}{N_b}\theta''_{m-1} + \sum_{k=0}^{m-1} f_{m-1-k}\phi'_k - S_r, \quad (43)$$

$$\overset{\chi}{m}(\xi) = \chi''_{m-1} - Pe \sum_{k=0}^{m-1} \chi_{m-1-k}\phi''_k + Pe * \Omega\phi''_{m-1} + Pe \sum_{k=0}^{m-1} \chi'_{m-1-k}\phi'_k + L_b \sum_{k=0}^{m-1} \chi'_{m-1-k}f_k, \quad (44)$$

$$\delta_m = \begin{cases} 0, & m \leqslant 1 \\ 1, & m > 1. \end{cases} \quad (45)$$

4. Results and Discussion

This work examined the effects of the transmission of warmth and mass on the flow of a heat-generating bioconvection Casson liquid. The permeability layer allows liquid to pass over a porous medium. The implications of Forchheimer's Rule are discussed. The dynamics of non-dimensional parameters in the context of temperature, velocity, and gyrotactic microorganism gradients are graphically depicted in the current setup. Figures explain how different factors affect the concentration of nanoparticles, temperature, velocities, and gyrotactic microbe distributions. The average values of the appropriate parameters are chosen in the Mathematica programme in the following way: $Nt = 0.10$, $M = 0.20$, P_m=.40, Nb=0.30, $Ec = 0.40$, $Pe = 0.30$, $\Omega = 0.30$, $D_a = 0.10$, $Q_0 = 0.30$, $Pr = 0.40$, $Pe = 0.40$ Bi= 0.4, Λ_1=0.2, F_r=0.3, S_r=0.3 and $Lb = 0.40$. The initial effect in the current mechanism is represented by the blue curve; the final behaviour of the profile, which alternates between raising and diminishing, is shown by the black, red, and magenta variations.

4.1. Velocity Profile

In this part, discuss several parameters linked to the velocity of the Casson nanofluid. The actions of the velocity components $f'(\xi)$ as a consequence of β, M, and P_m are shown in Figures 9, 10, 11. The implication of the β on the velocity profile $f'(\xi)$ is shown in Figure 9. Estimates of β in this case vary from 0.2 to 0.8, which reduces fluid velocity. Physically, when the β surges, the release pressure of the Casson liquid drops, increasing its flexible fluid viscosity. This causes a decline in the rate of movement on the porosity-extended surface of the Casson nanofluid. The flowing inclination of the nanoparticle's viscosity is responsible for the velocity profile's decreasing traits as β climbs. Figure 10 illustrates how the $f'(\xi)$ responds when M is applied. In physical terms, a magnetic field applied straight on the liquid produces the famous drag force, also known as the Lorentz force. Through a stretching sheet, the Lorentz effect can lessen the motion of the nanoparticles. A strong magnetic field applied perpendicular to a porous stretched sheet is the reason for it. Strong empirical values of P_m are linked to a spike in Casson liquid flow rate via permeable spreadsheets, as demonstrated through the physical impact of the porosity on the $f'(\xi)$, as illustrated in Figure 11. The flow play is higher due to the pores in the porous medium over the stretch sheet.

 doi:10.20944/preprints202503.0250.v1

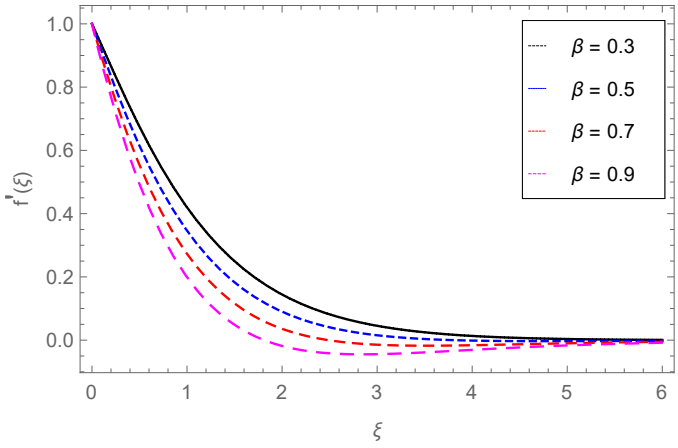

Figure 9. The influence of β on the velocity profile.

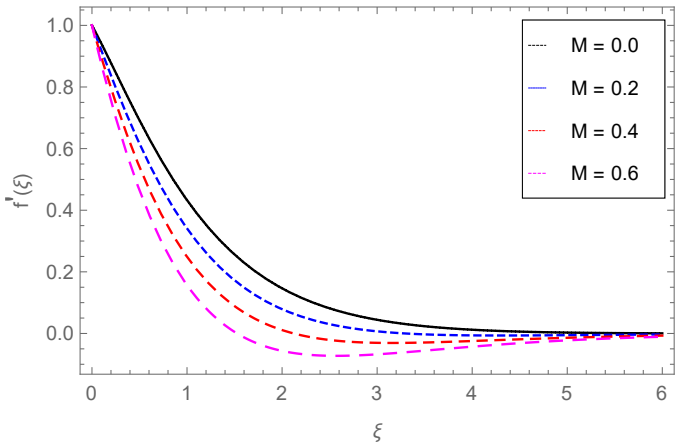

Figure 10. The influence of M on the velocity profile.

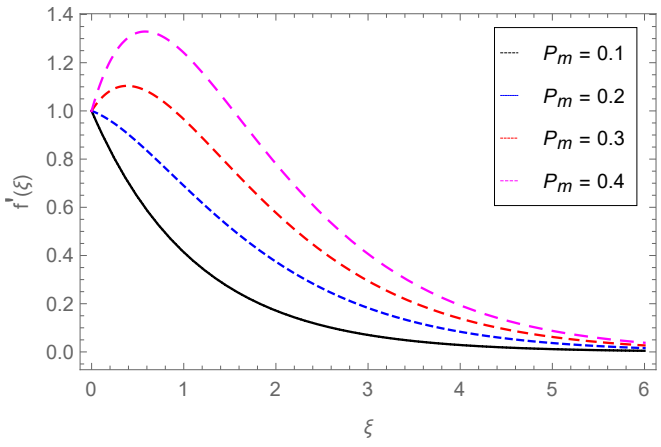

Figure 11. The influence of P_m on the velocity profile.

 doi:10.20944/preprints202503.0250.v1

4.2. Temperature Profile

Thermal curves with different parameters are explained in detail in this section. The implications of thermal energy on swimming germs across the porous surface are discussed here. Some germs died due to the extreme heat. Some living things endure temperatures as high as freezing, but most can't endure conditions that are either incredibly hot or very cold. As can be shown in Figure 12, alterations to the *Nb* amount cause a rise in the efficiency of the thermal field. This happens due to the temperature $\theta(\xi)$ enhancement allowed the tiny particles to collide more often. Physically, there is a discernible mobility of the nanomaterials in response to an increase in *Nb*, which increases their rate of motion and increases their heat-producing capacity. Figure 13 illustrates the consequence of *Ec* on the temperature description, which displays a rising profile as *Ec* values climb. This is because there is a lot greater movement of liquid particles across the sheet interface because of the close connection between the Eckert value and kinetic energy. Physically, large estimations of Eckert number Ec friction force are produced. As a result of the increased heat dissipation due to friction force. The influence of *Fr* on the thermal gradient is shown in Figure 14. Since the *Fr* factor occurs, the warmth curve to the sheet area shows an enhanced pattern. Physically, a procedure called thermophoresis transfers tiny molecules from a warm to a cooled one. A rise in *Nt* generates a higher thermophoretic power, which encourages more nanoparticles to migrate from a hot to a cool surrounding fluid. This increases the temperature influx and raises the temperature of the width, supporting the idea. Figure 15 emphasises the importance of the Casson nanofluid in the framework, showing how raising the value of *Pr* improves thermal transport. By transferring a significant quantity of thermal power through the surface to the substance, the warmth-generating process raises the substance's warmth within the blade BL area. Due to the reverse relationship between *Pr* and thermal dispersion, the effect is particularly noticeable at higher *Pr* since the temperature rate rises as BL depth. The influence of Q_0 on the temperature distribution is shown in Figure 16. Notice that heat exceeds due to variation inQ_0. The Casson liquid's response to the chemical reaction is depicted in Figure 17. In this case, chemical interactions improve the diffusion of heat. The temperature grows as thermophoresis values *Nt* increase, as Figure 18 exhibits. Improved heat transfer is achieved through a stronger thermophoresis diffusion impact, transferring a particle's heated half to a colder area. Figure 19 illustrates the extent of the D_a impact on the temperature. Thermal BL in the current stream diminishes as the Darcy number climbs. The ratio of viscosity to momentum in the movement of fluid via a porous medium is indicated by the Darcy number. Physically, a higher Darcy number indicates a stronger viscosity compared to inertial stress. The impact of the heat conductivity factor on the temperature gradient is displayed in Figure 20. In this case, it illustrates how the heat gradient moves beyond the sheet's surface, and its thermal layer increases as the value of Λ_1 grows.

 doi:10.20944/preprints202503.0250.v1

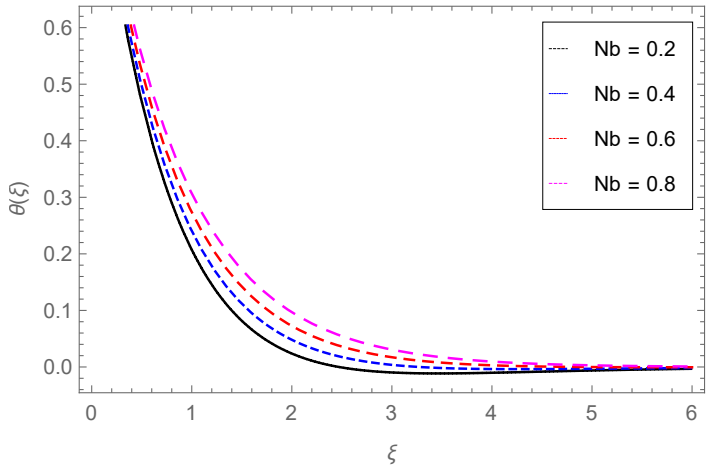

Figure 12. The influence of *Nb* on the temperature profile.

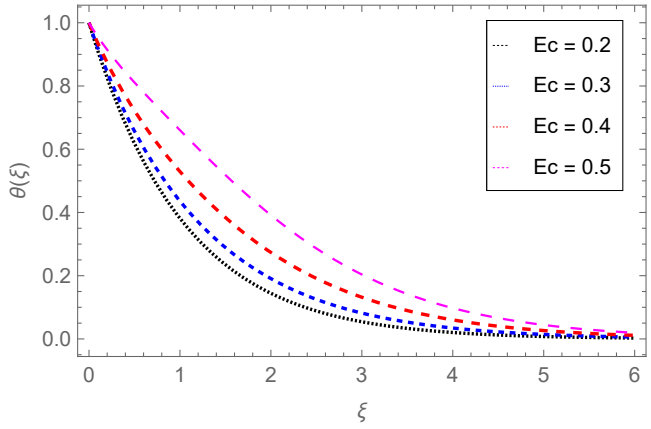

Figure 13. The influence of *Ec* on the temperature profile.

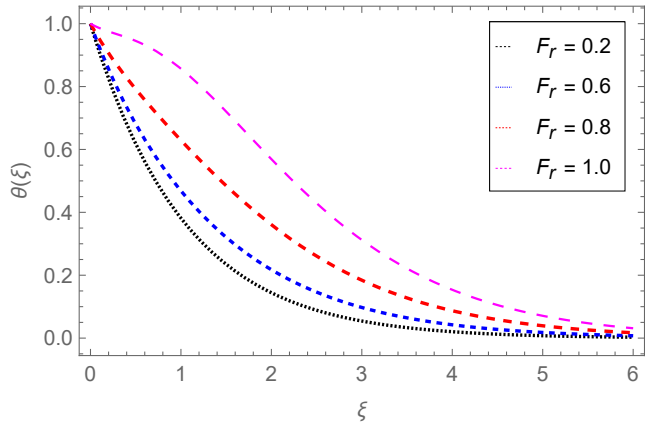

Figure 14. The influence of *Fr* on the temperature profile.

 doi:10.20944/preprints202503.0250.v1

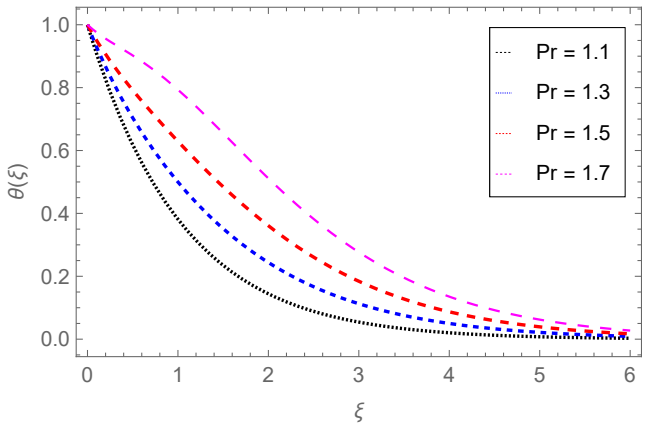

Figure 15. The influence of Pr on the temperature profile.

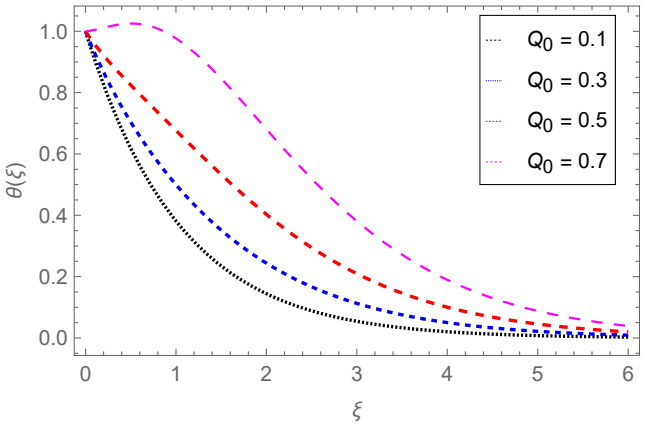

Figure 16. The influence of Q_0 on the temperature profile.

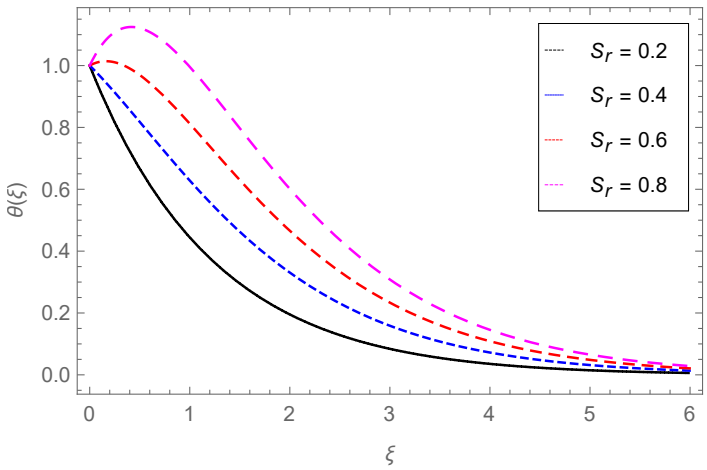

Figure 17. The influence of S_r on the temperature profile.

 doi:10.20944/preprints202503.0250.v1

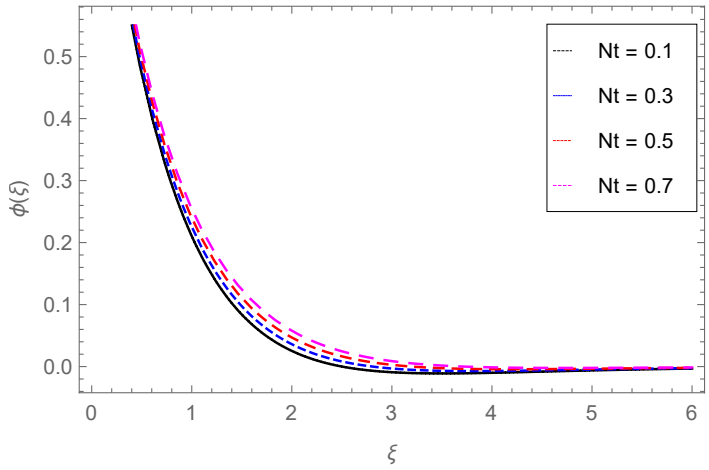

Figure 18. The influence of Nt on the temperature profile.

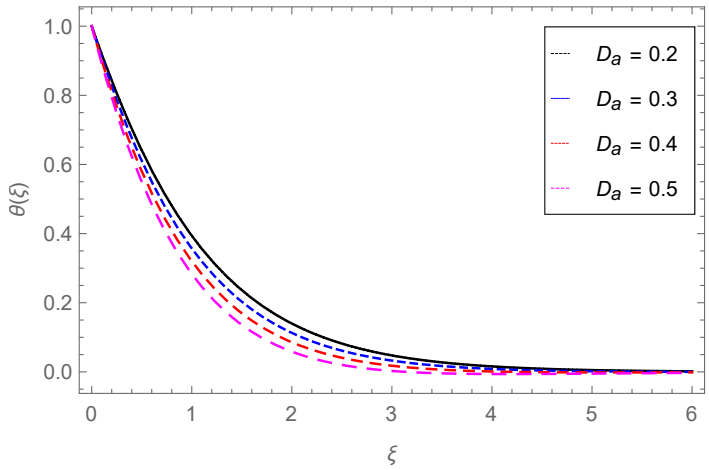

Figure 19. The influence of D_a on the temperature profile.

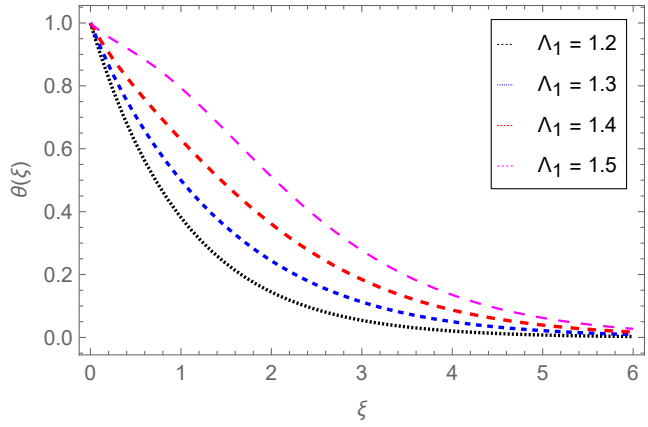

Figure 20. The influence of Λ_1 on the temperature profile.

 doi:10.20944/preprints202503.0250.v1

4.3. Concentration Profile

This section discusses the concentration distribution of the nanoparticles for multiple parameters and their physical behavior. Higher Nb significantly boosts the concentration profile $\phi(\xi)$. Physically, the movement of the nanoparticles across the fluid sheet is chaotic or random. The liquid particles travel irregularly and become intensively mixed, and the concentration field $\phi(\xi)$ upgrades, as reflected in Figure 21. The impact of the thermophoresis parameter Nt on the concentration trend is seen in Figure 22. With different values of the parameter Nt, the concentration of nanoparticles increases. The physical aspect of the thermophoresis scenario entails the transfer of nanoparticles from a heated region to a cooled region due to temperature variations. Figure 23 shows how variations in the Darcy parameter D_a impact the concentration profile. It shows that both the intensity pattern and the overall thickness of the BL decrease with an upsurge in the D_a parameter. The $\phi(\xi)$ versus the chemical response factor S_r for a stretched surface is shown in Figure 24. The chemical process has the potential to intensify intermolecular collisions; the structure's thermal production rises, and significantly more concentration is used. As the values of chemical responses increase, the pattern of concentration falls can be seen in Figure 24. Physically, chemical reaction drops $\phi(\xi)$ and accelerates the velocity at which source species break down.

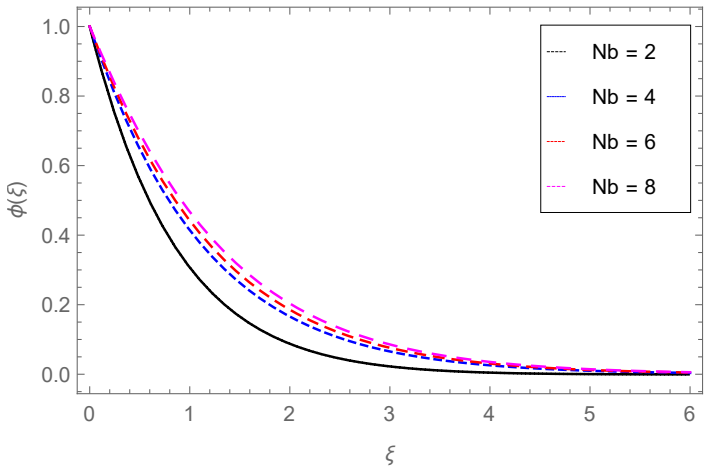

Figure 21. The influence of Nb on the concentration profile.

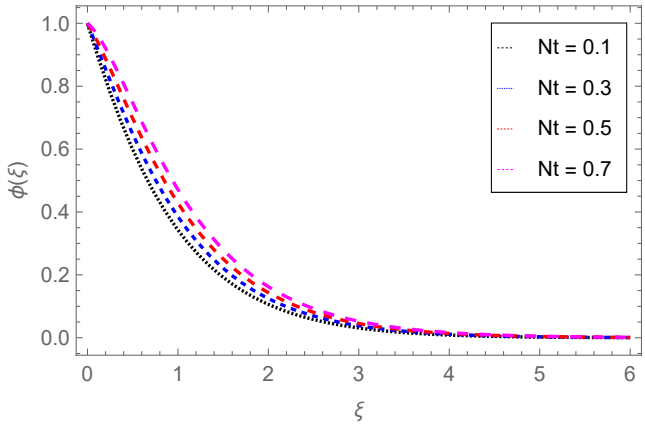

Figure 22. The influence of Nt on the concentration profile.

 doi:10.20944/preprints202503.0250.v1

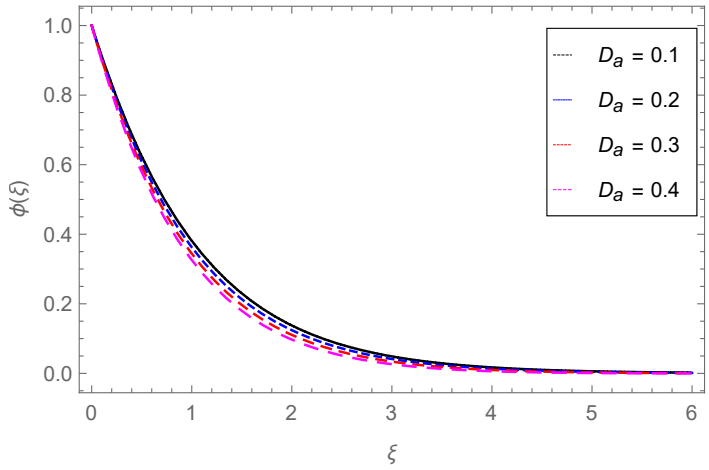

Figure 23. The influence of D_a on the concentration profile.

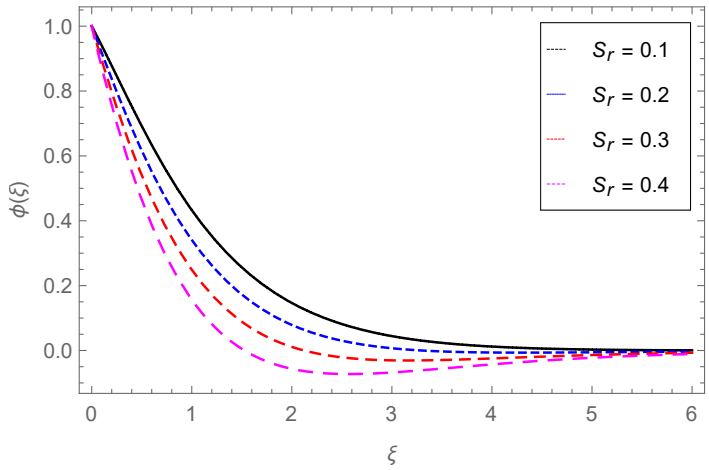

Figure 24. The influence of S_r on the concentration profile.

4.4. Gyrotactic Microorganism Profile

This section provides a thorough explanation of microorganism curves with various parameters. Figure 25 shows the behavior of the concentration of the gyrotactic microbe versus the bioconvection Lewis number *Lb*. Physically, the cooperative swimming of microorganisms, referred to as bioconvection, causes variations in density. Increasing the bioconvection Lewis number *Lb* has improved the diffusion rate and concentration of gyrotactic microorganisms, as displayed in Figure 25. Similarly, the greater *Pe* declined the concentration of gyrotactic microbes $\chi(\xi)$ significantly, as shown in Figure 26. Physically, the *Pe* is directly proportional to cell swimming motion and has an inverse relation with density. When the *Pe* number increases, the concentration of the gyrotactic microbe is enhanced on the stretching surface, but the density of the microbes is reduced. Figure 27 shows the action of the gyrotactic microbe spectrum as an expression of variable Ω fluctuation. The gyrotactic microbial population gets reduced through the large estimations of the concentration variation factor. Figure 28 depicts the dynamics of the gyrotactic microbe curve with the Schmidt constant. Notice that gyrotactic bacteria expanded as the *Sc* climbed due to the dynamic viscosity improving as the *Sc* varied.

 doi:10.20944/preprints202503.0250.v1

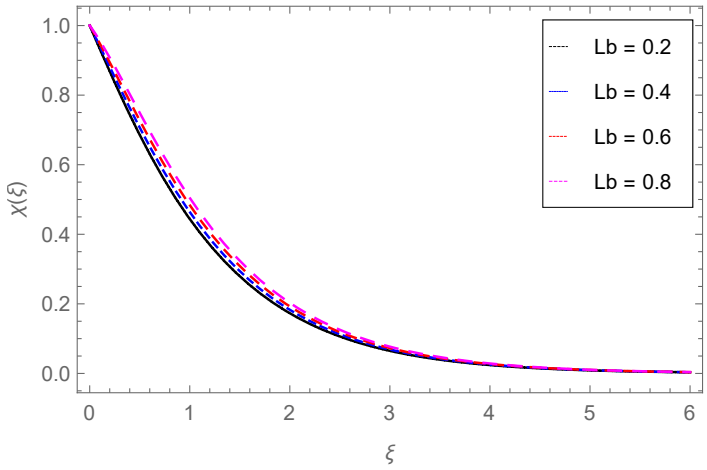

Figure 25. The influence of *Lb* on the gyrotactic microorganism profile.

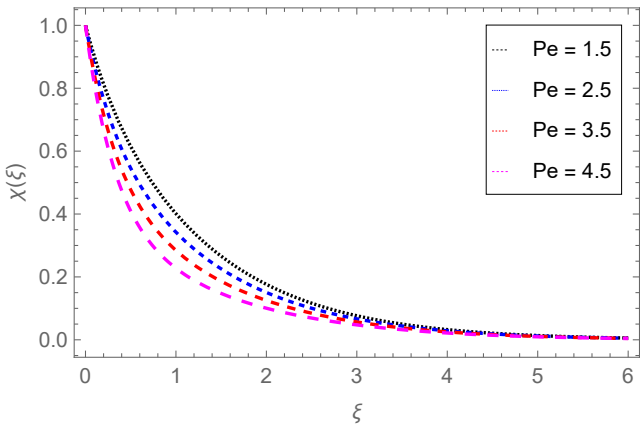

Figure 26. The influence of *Pe* on the gyrotactic microorganism profile.

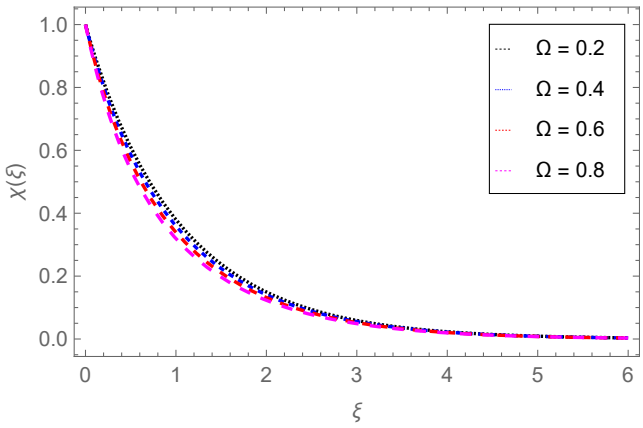

Figure 27. The influence of Ω on the gyrotactic microorganism profile.

 doi:10.20944/preprints202503.0250.v1

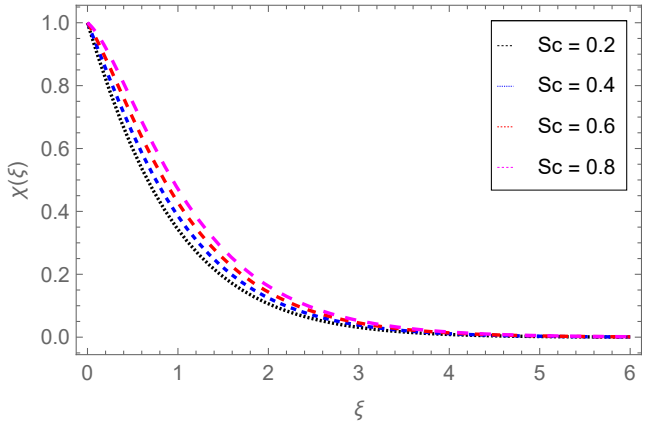

Figure 28. The influence of Sc on the gyrotactic microorganism profile.

4.5. Remarks on Contrasting the Current Collection of Work Against [70].

The comparison between shooting and HAM is shown in Figures 29– 32. Each of the techniques is most compatible with one another. To confirm the validity and dependability of the observable analytical structure, the HAM results are further compared with earlier studies. Table 1 presents numerical results that replicate the impacts of several parameters on skin friction coefficient, the Nusselt number and Shoord number, namely the magnetic field parameter M, Casson parameter β, Biot number Bi, Forchheimer parameter F_r, and Darcy parameter D_a, as well as the Eckert numbers Ec and Pr. The details collected from the current work employing the homotopy analysis technique are entirely consistent with results obtained using the shooting method that have already been published [70].

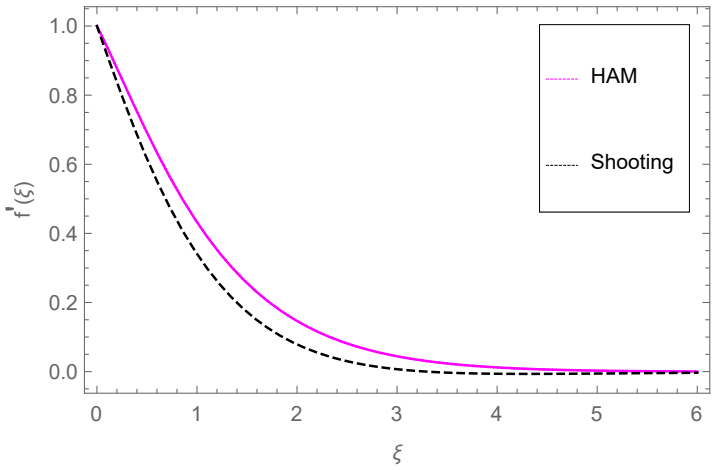

Figure 29. Velocity profile.

 doi:10.20944/preprints202503.0250.v1

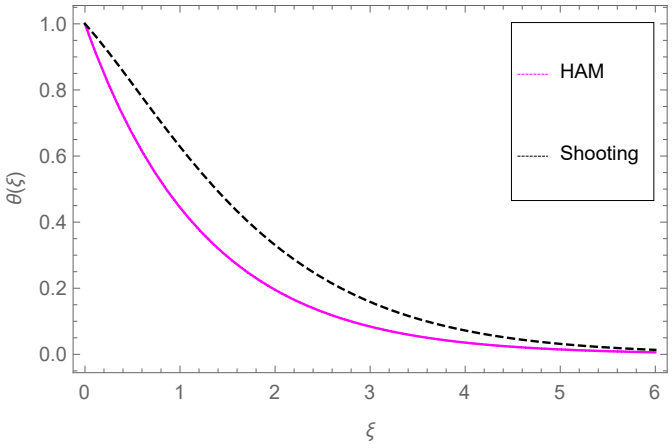

Figure 30. Temperature profile.

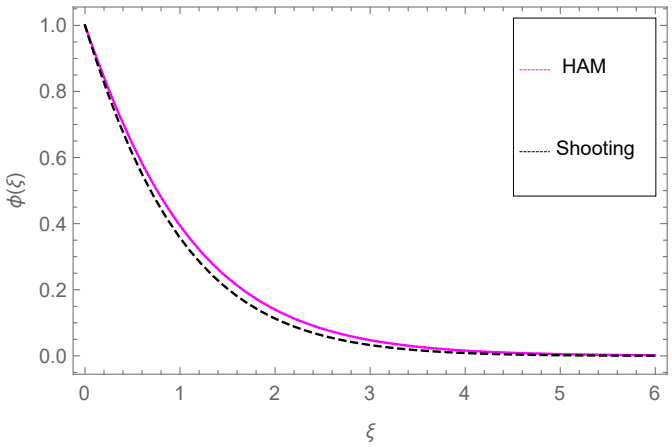

Figure 31. Nanoparticles concentration profile.

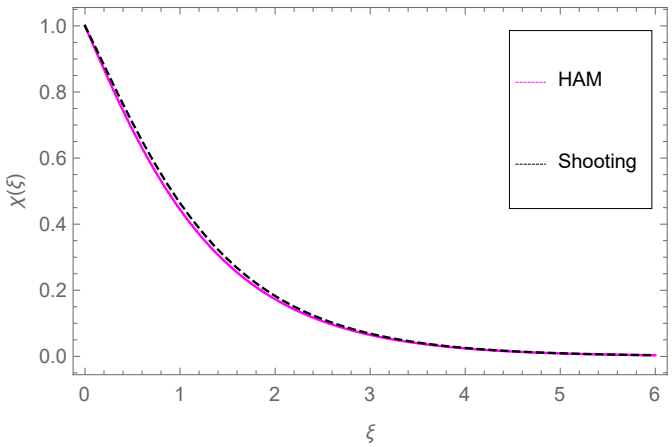

Figure 32. Gyrotactic miroorganisms profile.

 doi:10.20944/preprints202503.0250.v1

Table 1. Performance of the C_{f_x}, Nu_x, and Sh_x to show the comparison with published work [70].

$\sqrt{(Re_x)}C_{f_x}$	Presents results	$\sqrt{(Re_x)}Nu_x$	Presents results	$\sqrt{(Re_x)}Sh_x$	Presents results
1.51502	1.51501	0.0928714	0.0928711	0.825845	0.825840
1.66663	1.66661	0.0923999	0.0923994	0.806926	0.806923
1.89542	1.89543	0.0916227	0.0916225	0.779026	0.779022
1.83257	1.83255	0.0906326	0.0906323	0.786406	0.786401
1.70039	1.70034	0.0920388	0.0920386	0.802712	0.802710
1.66663	1.66655	0.0923999	0.0923998	0.806926	0.806925
1.66663	1.66658	0.0923999	0.0923994	0.806926	0.806922
1.76956	1.76959	0.0912866	0.0912863	0.796401	0.796402
1.85492	1.85490	0.0903812	0.0903807	0.787746	0.787744
2.76472	2.76471	0.0873642	0.0873640	0.886156	0.886153
1.66663	1.66661	0.0923999	0.0923978	0.806926	0.806924
1.21544	1.21542	0.0941238	0.0941237	0.766893	0.766890
1.67388	1.67385	0.0924106	0.0924104	0.807306	0.807302
1.62478	1.62467	0.0923341	0.0923342	0.804575	0.804572
1.56035	1.56027	0.0922204	0.0922201	0.800409	0.800404
1.88054	1.88053	0.0921267	0.0921265	0.809828	0.809824
1.66663	1.66662	0.0923999	0.0923996	0.806926	0.806925
1.46167	1.46165	0.0926254	0.0926253	0.801361	0.801362
1.55498	1.55497	0.0900135	0.0900132	0.563252	0.563251
1.66663	1.66662	0.0923999	0.0923993	0.806926	0.806924
1.90001	1.90002	0.0952221	0.0952220	1.397651	1.397650
1.66663	1.66662	0.0923999	0.0923996	0.806926	0.806924
1.66566	1.66559	0.265119	0.265105	0.806856	0.806854
1.66476	1.66472	0.4234431	0.4234425	0.806791	0.806792
1.66665	1.66658	0.0924475	0.0924470	0.806928	0.806926
1.66634	1.66632	0.0919339	0.0919331	0.806913	0.806912
1.66575	1.66573	0.0909649	0.0909645	0.806884	0.806882

5. Conclusions and Final Remarks

The scientific and analytical investigation of biological convection Casson nanofluid circulation resulting from sheet stretch has been the focus of the current work. Via chemical reactions and Darcy-Forchheimer flow in porous media. This work is distinctive because it offers a discussion of the phenomena of Casson fluid flow, including the intricate relationships among heating sources, chemical reactions, heat barrier layer, permeation, and viscous dispersion, as well as the implications of Darcy number and Forchheimer law. The results of this work are highly significant in terms of practical engineering cooling applications as well as theoretical advances in the mathematical modeling of Casson fluid flow with heat mass transfer in engineering systems. The findings of this study have a significant impact on both practical applications of cooling and theoretical developments in the mathematical simulation of Casson liquid movement with heat exchange in engineered frameworks. Some of the most important results from the current study are as follows:

- The velocity profile falls with M and β, while fluid movement is enhanced through the porous parameter P_m.
- The temperature profile increases with Nb, Ec, Pr, S_r, Nt, Q_0, F_r, and Λ_1, while it is reduced through the Darcy parameter D_a.
- The concentration of nanoparticles is enhanced with Nb, Nt but reduced against the Darcy parameter D_a and chemical reactions S_r.
- The concentration of gyrotactic microbes is raised with Lb, Pe, Sc but reduced with the concentration difference parameter Ω.

Funding: No funding is received for conducting this study.

 doi:10.20944/preprints202503.0250.v1

Data Availability Statement: Data will be made available on request.

Conflicts of Interest: The author has no financial and personal relationships with other people or organizations that could inappropriately influence (bias) his work. i.e. conflict of interest is none.

Nomenclature

M	Magnetic field parameter	Ω	Concentration difference parameter
Nt	Thermophoresis parameter	Nb	Brownian motion parameter
W_{ce}	Maximum cell swimming speed	Lb	Bioconvection Lewis number
Pr	Prandtl number	Ec	Eckert number
B_0	Magnetic field strength	T_∞	Ambient temperature (k)
N	Concentration of microorganisms	(u,v)	Components of velocity (ms^{-1})
D_T	Thermophoretic diffusion coefficient	C_∞	Ambient concentration
b	Chemotaxis constant	C_w	Surface concentration
T	Fluid temperature (k)	C	Concentration
D_B	Brownian diffusion coefficient	T_w	Temperature on wall (k)
D_n	Diffusion of microbes	f	Velocity profile
a	Dimensional constant	N_∞	Ambient concentration of microbes
c_p	Specific heat at constant pressure	(x,y)	Axis coordinates (m)
k_p	Thermal conductivity	N_w	Reference concentration of microbes
(a, b)	Dimensional constants	Pe	Bioconvection Peclet number
Bi	Biot number	C_{f_x}	Skin friction coefficient
P_m	Porosity parameter	Sc	Schmidt number
D_a	Darcy parameter	F_r	Forchheimer parameter
Q_0	Heat source parameter	S_r	Chemical reaction
Greek Letters			
μ	Dynamic viscosity of nanopartcles	ν	Kinematic viscosity of nanopartcles
ρ	Density of nanoparticle(kgm^3)	σ	Electrical conductivity
ξ	Similarity variable	τ	Stefan Boltzmann Constant fluid
ϕ	Concentration profile	θ	Temperature profile
β	Casson fluid parameter	χ	Gyrotactic microorganisms profile
λ	Stretching ratio parameter	μ_1	Plastic dynamic viscosity

References

1. Alwawi, F.A., Alkasasbeh, H.T., Rashad, A.M., Idris, R.: MHD natural convection of sodium alienate Casson nanofluid over a solid sphere. Results in Physics. 16, 102818 (2020).
2. Mukhopadhyay, S.: Effects of thermal radiation on Casson fluid flow and heat transfer over an unsteady stretching surface subjected to suction/blowing. Chinese Physics B. 22(11), 114702 (2013).
3. Mabood, F., Das, K.: Outlining the impact of melting on MHD Casson fluid flow past a stretching sheet in a porous medium with radiation. Heliyon. 5(2), e01216 (2019).
4. Shah, Z., Kumam, P., Deebani, W.: Radiative MHD casson nanofluid flow with activation energy and chemical reaction over past nonlinearly stretching surface through Entropy generation. Scientific Report. 10, 4402 (2020).
5. Puneeth, V., Khan, M.I., Narayan, S.S., El-Zahar, E.R., Guedri, K.: The impact of the movement of the gyrotactic microorganisms on the heat and mass transfer characteristics of Casson nanofluid. Waves Random Complex Media. 1–24 (2022).
6. Nadeem, S., Haq, R.U., Lee, C.: MHD Flow of a Casson Fluid over an Exponentially Shrinking Sheet. Scientia Iranica. 19, 1550-1553 (2012).
7. Alali, E., Megahed, A.M.: MHD dissipative Casson nanofluid liquid film flow due to an unsteady stretching sheet with radiation influence and slip velocity phenomenon. Nanotechnology. Rev. 11, 463– 472 (2022).
8. Dawar, A., Shah, Z., Alshehri, H.M., Islam, S., Kumam, P.: Magnetized and nonmagnetized Casson fluid flow with gyrotactic microorganisms over a stratified stretching cylinder. Sci Rep. 11, 16376 (2021).

 doi:10.20944/preprints202503.0250.v1

9. Mkhatshwa, M.P., Motsa, S., Sibanda, P.: MHD bioconvective radiative flow of chemically reactive Casson nanofluid from a vertical surface with variable transport properties. Int. J. Ambient Energy. 43, 3170-3188 (2020).
10. Darcy, H.P.C.: Les Fontsines Publiques de la Ville de Dijon. Victor Dalmont, Paris. (1856)
11. Li, S., Raghunath, K., Alfaleh, A., Ali, F., Zaib, A., Khan L.M.: Effects of activation energy and chemical reaction on unsteady MHD dissipative Darcy-Forchheimer squeezed flow of Casson fluid over horizontal channel. Sci Rep. 13(1), 2666 (2023).
12. Nayak, M.K., Shaw, S., Khan, M.I., Makinde, O., Chu, Y.M., Khan, S.U.: Inter-facial layer and shape effects of modified Hamilton's Crosser model in entropy optimized Darcy–Forchheimer flow. Alex. Eng. J. 60, 4067–4083 (2021).
13. Bilal, S., Sohail, M., Naz, R.: Heat transport in the convective Casson fluid flow with homogeneous heterogeneous reactions in Darcy-Forchheimer medium, Multidiscip. Model. Mater. Struct. 15, 1170–1189 (2019).
14. Naz, R., Tariq, S., Sohail, M., Shah, Z.: Investigation of entropy generation in stratified MHD Carreau nanofluid with gyrotactic microorganisms under Von Neumann similarity transformations, Eur. Phys. J. Plus. 135, 1–22 (2020).
15. Naz, R., Mabood, F., Sohail, M., Tlili, I.: Thermal and species transportation of Eyring-Powell material over a rotating disk with swimming microorganisms: applications to metallurgy. J. Mater. Res. Technol. 9, 5577–5590 (2020).
16. Rasool, G., Shah, N.A., El-Zahar, E.A., Wakif, A.: Numerical investigation of EMHD nanofluid flows over a convectively heated riga pattern positioned horizontally in a Darcy-Forchheimer porous medium: Application of passive control strategy and generalized transfer laws. Waves Random Complex Media. 1–20 (2022).
17. Kairi, R.R., Shaw, S., Roy, S., Raut, S.: Thermosolutal marangoni impact on bioconvection in suspension of gyrotactic microorganisms over an inclined stretching sheet. J. Heat Transf. 143, 031201 (2021).
18. Mkhatshwa, M.P., Motsa, S., Sibanda, P.: MHD bioconvective radiative flow of chemically reactive Casson nanofluid from a vertical surface with variable transport properties. Int. J. Ambient. Energy. 43, 3170-3188 (2020).
19. Farooq Waqas, U., Shah, H., Kumam, Z., Deebani, W.P.: On unsteady 3D bioconvection flow of viscoelastic nanofluid with radiative heat transfer inside a solar collector plate. Sci Rep. 12, 2952 (2022).
20. Mahdy, A.: Natural convection boundary layer flow due to gyrotactic microorganisms about a vertical cone in porous media saturated by a nanofluid. J Brazil Soc Mech Sci Eng. 38, 67-70 (2015).
21. Giri, S.S., Das, K., Kundu, P.K.: Stefan blowing effects on MHD bioconvection flow of a nanofluid in the presence of gyrotactic microorganisms with active and passive nanoparticles flux. Eur Phys J Plus. 132, 101 (2017).
22. Waqas, H., Farooq, U., Shah, Z., Kumam, P., Shutaywi, M.: Second-order slip effect on bio-convectional viscoelastic nanofluid flow through a stretching cylinder with swimming microorganisms and melting phenomenon. Sci Rep. 11, 11208 (2021).
23. Khan, N.S., Shah, Q., Sohail, A.: Dynamics with Cattaneo–Christov heat and mass flux theory of bioconvection Oldroyd-B nanofluid. Adv Mech Eng. 12(7), 16–20 (2020).
24. Khan, N.S., Humphries, U.W., Kumam, W., Kumam, P., Muhammad, T.: Bioconvection Casson nanoliquid film sprayed on a stretching cylinder in the portfolio of homogeneous-heterogeneous chemical reactions. ZAMM Angew Math Mech. 101(102), (2022) e202000212.
25. Khan, N.S., Humphries, U.W., Kumam, W., Kumam, P., Muhammad, T.: Dynamic pathways for the bioconvection in thermally activated rotating system. Biomass Conver Bioref. 14 (7), 8605-8623 (2022).
26. Khan, N.S., Shah, Z., Islam, S., Khan, I., Alkanhal, T.A., Tlili, I.: Entropy generation in MHD mixed convection non-Newtonian second-grade nanoliquid thin film flow through a porous medium with chemical reaction and stratification. Entropy. 21(2), 139 (2019).
27. Zuhra, S., Khan, N.S., Islam, S.: Magnetohydrodynamic second grade nanofluid flow containing nanoparticles and gyrotactic microorganisms. Comp Appl Math. 37, 6332–58 (2018).
28. Palwasha, Z., Islam, S., Khan, N.S., Hayat, H.: Non-Newtonian nanoliquids thin film flow through a porous medium with magnetotactic microorganisms. Appl Nanosci. 8, 1523–44 (2018).

 doi:10.20944/preprints202503.0250.v1

29. Sajid, M., Iqbal, S.A., Naveed, M., Abbas, Z.: Effect of homogeneousheterogeneous reactions and magnetohydrodynamics on Fe_3O_4 nanofluid for the Blasius flow with thermal radiations. J Mol Liq. 233, 115–21 (2017).
30. Sravanthi, C.S., Mabood, F., Nabi, S.G., Shehzad, S.A.: Heterogeneous and homogeneous reactive flow of magnetite-water nanofluid over a magnetized moving plate. Propulsion Power Res. 11(2), 265–75 (2022).
31. Alzahrani, F., Gowda, R.J.P., Kumar, R.N., Khan, M.I.: Dynamics of thermosolutal Marangoni convection and nanoparticle aggregation effects on Oldroyd-B nanofluid past a porous boundary with homogeneous-heterogeneous catalytic reactions. J Indian Chem Soc. 99(6), 100458 (2022).
32. Mabood, F., Nayak, M.K., Chamkha, A.J.: Heat transfer on the cross flow of micropolar fluids over a thin needle moving in a parallel stream influenced by binary chemical reaction and Arrhenius activation energy. Eur. Phys. J. Plus. 134(9), 427 (2019).
33. Ramzan, M., Shaheen, N., Kadry, S., Ratha, Y., Nam, Y.: Thermally stratified darcy forchheimer flow on a moving thin needle with homogeneous heterogeneous reactions and non-uniform heat source/sink. Appl. Sci. 10(2), 432 (2020).
34. Makinde, O.D., Animasaun, I.L.: Thermophoresis and Brownian motion effects on MHD bioconvection of nanofluid with nonlinear thermal radiation and quartic chemical reaction past an upper horizontal surface of a paraboloid of revolution. J. Mol. Liq. 221, 733–743 (2016).
35. Khan, M.I., Waqas, M., Hayat, T., Alsaedi, A.: A comparative study of Casson fluid with homogeneous-heterogeneous reactions. J. Colloid Interface Sci. 498, 85–90 (2017).
36. Hamid, A.: Terrific effects of Ohmic-viscous dissipation on Casson nanofluid flow over a vertical thin needle: Buoyancy assisting and opposing flow. J. Mater. Res. Technol. 9(5), 11220–11230 (2020).
37. Dawar, A., Acharya, N.: Unsteady mixed convective radiative nanofluid flow in the stagnation point region of a revolving sphere considering the influence of nanoparticles diameter and nanolayer. J. Indian Chem. Soc. 99(10), 100716 (2022).
38. Acharya, N., Mabood, F., Badruddin, I.A.: Thermal performance of unsteady mixed convective Ag/MgO nanohybrid flow near the stagnation point domain of a spinning sphere. Int. Commun. Heat Mass Transf. 134, 106019 (2022).
39. Acharya, N., Mabood, F., Shahzad, S.A., Badruddin, I.A.: Hydrothermal variations of radiative nanofluid flow by the influence of nanoparticles diameter and nanolayer. Int. Commun. Heat Mass Transf. 130, 105781 (2022).
40. Acharya, N.: Spectral simulation to investigate the effects of nanoparticle diameter and nanolayer on the ferrofluid flow over a slippery rotating disk in the presence of low oscillating magnetic field. Heat Transf. 50(6), 5951–5981 (2021).
41. Acharya, N.: Framing the impacts of highly oscillating magnetic field on the ferrofluid flow over a spinning disk considering nanoparticle diameter and solid–liquid interfacial layer. J. Heat Transf. 142(10), 102503 (2020).
42. Khan, N.S., Zuhra, S., Shah, Q.: Entropy generation in two phase model for simulating flow and heat transfer of carbon nanotubes between rotating stretchable disks with cubic autocatalysis chemical reaction. Appl Nanosci. 9, 1797–822 (2019).
43. Dawar, A., Shah, Z., Tassaddiq, A., Kumam, P., Islam, S., Khan, W.: A convective flow of Williamson nanofluid through cone and wedge with non-isothermal and non-isosolutal conditions: A revised buongiorno model. Case Stud Therm Eng. 24, 100869 (2021).
44. Cao, W., Lare, A.I., Yook, S.J., Ji, X.: Simulation of the dynamics of colloidal mixture of water with various nanoparticles at different levels of partial slip. Ternary-hybrid nanofluid. Int Commun Heat Mass Transfer. 135, 106069 (2022).
45. Alrabaiah, H., Bilal, M., Khan, M.A., Muhammad, T., Legas, E.Y.: Parametric estimation of gyrotactic microorganism hybrid nanofluid flow between the conical gap of spinning disk-cone apparatus. Sci Rep. 12, 59 (2022).
46. Nazir, U., Sohail, M., Selim, M.M., Alrabaiah, H., Kumam, P.: Finite element simulations of hybrid nano-Carreau Yasuda fluid with hall and ion slip forces over rotating heated porous cone. Sci Rep. 11, 19604 (2021).
47. Shahid, N., Rana, M., Siddique, I.: Exact solution formotion of an Oldroyd-B fluid over an infinite flat plate that applies an oscillating shear stress to the fluid. Bound Value Prob. 10, 48 (2012).

 doi:10.20944/preprints202503.0250.v1

48. Oke, A.S.: Combined effects of Coriolis force and nanoparticle properties on the dynamics of gold-water nanofluid across nonuniform surface. ZAMM Angew Math Mech. e202100113 (2022) .
49. Liu, B., Yang, W., Liu, Z.: A PANS method based on rotation-corrected energy spectrum for efficient simulation of rotating flow. Front Energ Res. 10, 894258 (2022).
50. Ali, B., Shafiq, A., Siddique, I., Al-Madallal, Q., Jarad, F.: Significance of suction/ injection, gravity modulation, thermal radiation, and magnetohydrodynamic on dynamics of micropolar fluid subject to an inclined sheet via finite element approach. Case Stud Therm Eng. 28, 101537 (2021).
51. Lei, T., Siddique, I., Ashraf, M.K., Hussain, S., Abdal, S., Ali, B.: Computational analysis of rotating flow of hybrid nanofluid over a stretching surface. Proceed Inst Mechl Eng E: J Process Mech Eng. 236(6), 095440892211000 (2022).
52. Habib, D., Salamat, N., Abdal, S., Siddique, I., Salimi, M., Ahmadian, A.: On time dependent MHD nanofluid dynamics due to enlarging sheet with bioconvection and two thermal boundary conditions. Microfluid Nanofluid. 26, 11 (2022).
53. Hussain, F., Nazeer, M., Ghafoor, I., Saleem, A., Waris, B., Siddique, I.: Perturbation solution of Couette flow of casson nanofluid with composite porous medium inside a vertical channel. Nano Sci Technol Int J. 13(4), 23–44 (2022).
54. Siddique, I., Zulqarnain, R.M., Nadeem, M., Jarad, F.: Numerical simulation of MHD Couette flow of a Fuzzy nanofluid through an inclined channel with thermal radiation effect. Comput Intell Neurosci. 6608684, 1–16 (2021).
55. Abdal, S., Siddique, I., Saif Ud Din, I., Ahmadian, A., Hussain, S., Salimi, M.: Significance of magnetohydrodynamic Williamson Sutterby nanofluid due to a rotating cone with bioconvection and anisotropic slip. ZAMM Angew Math Mech. e202100503 (2022).
56. Sadiq, K., Siddique, I., Ali, R., Jarad, F.: Impact of ramped concentration and temperature on MHD Casson nanofluid flow through a vertical channel. J. Nanomater. 3743876, 1–17 (2021).
57. Iqbal, S., Siddique, I., Siddiqui, A.M.: OHAM and FEM solutions of concentric n-layer flows of incompressible third-grade fluids in a horizontal cylindrical pipe. J. Braz Soc Mech Sci Eng. 41, 204 (2019).
58. Song, Y.Q., Obideyi, B.D., Shah, N.A., Animasaun, I.L., Mahrous, Y.M., Chung, J.D.: Significance of haphazard motion and thermal migration of alumina and copper nanoparticles across the dynamics of water and ethylene glycol on a convectively heated surface. Case Stud Therm Eng. 26, 101050 (2021).
59. Oke, A.S., Animasaun, I.L., Mutuku, W.N., Kimathi, M., Shah, N.A, Saleem, S.: Significance of Coriolis force, volume fraction, and heat source/sink on the dynamics of water conveying 47 nm alumina nanoparticles over a uniform surface. Chin J Phys. 71, 716–27 (2021).
60. Khan, N.S., Shah, Q., Bhaumik, A., Kumam, P., Thounthong, P., Amiri, I.: Entropy generation in bioconvection nanofluid flow between two stretchable rotating disks. Sci Rep. 10, 4448 (2020).
61. Usman, A.H., Khan, N.S., Rano, S.A., Humphries, U.W., Kumam, P.: Computational investigations of Arrhenius activation energy and entropy generation in a viscoelastic nanofluid flow thin film sprayed on a stretching cylinder. J Adv Res Fluid Mech Therm Sci. 86(1), 27–51 (2021).
62. Ramzan, M., Khan, N.S., Kumam, P.: Mechanical analysis of non-Newtonian nanofluid past a thin needle with dipole effect and entropic characteristics. Sci Rep. 11(1), 19378 (2021).
63. Khan, N.S., Humphries, U.W., Kumam, W., Kumam, P., Muhammad, T.: Bioconvection Casson nanoliquid film sprayed on a stretching cylinder in the portfolio of homogeneous-heterogeneous chemical reactions. Z Angew Math Mech. 8, e2020000222 (2022).
64. L. Ali, Z. Omar, I. Khan, J. Raza, M. Bakouri, I. Tlili.: Stability analysis of Darcy-Forchheimer flow of Casson type nanofluid over an exponential sheet: investigation of critical points. Symmetry. 11, 412 (2019).
65. J. Kavita, S. Kalpna, P. Choudhary, P. Soni, A. Rifaqat, M. Ganesh. Significance of Darcy–Forchheimer Casson fluid flow past a non-permeable curved stretching sheet with the impacts of heat and mass transfer. Case Studies in Thermal Engineering. 61, 104907 (2024).
66. N.M. Hafez, E. N. Thabet, Zeeshan Khan, A.M. Abd-Alla, S.H. Elhag.: Electroosmosis-modulated Darcy-Forchheimer flow of Casson nanofluid over stretching sheets in the presence of Newtonian heating. Case Studies in Thermal Engineering. 53, 103806 (2024).
67. Shaw, S., Patra, A., Misra, A., Nayak, M.K.: Assisting/opposing/forced convection flow on entropy-optimized MHD nanofluids with variable viscosity. Interfacial layer and shape effects. Heat Transf. 51(1), 578–603 (2021).

 doi:10.20944/preprints202503.0250.v1

68. Himanshu, U., Priya, B., Kumar, P.A., Makinde, O.D.: Heat transfer assessment for Au-blood nanofluid flow in Darcy-Forchheimer porous medium using induced magnetic field and Cattaneo-Christov model. Numer Heat Transf. Part B. Fundamentals. 84(4), 415–31 (2023).
69. Satya Narayana, P.V., Tarakaramu, N., Moliya Akshit, S., Jati P.G.: MHD flow and heat transfer of an Eyring-Powell fluid over a linear stretching sheet with viscous dissipation-A numerical study. Front Heat Mass Transf. 9(1), 1–5 (2017).
70. Elgendi, S.G., Abbas, W.,· Ahmed, A.M.: Said,·A. M.: Megahed Eman Fares. Computational Analysis of the Dissipative Casson Fluid Flow Originating from a Slippery Sheet in Porous Media. Journal of Nonlinear Mathematical Physics. 31, 19 (2024).